CHEMISTRY

Gas-phase preparation of silylacetylene (SiH_3CCH) through a counterintuitive ethynyl radical (C_2H) insertion

Shane J. Goettl[1]†, Allen Vincent[1]†, Mateus X. Silva[2]‡, Zhenghai Yang[1], Breno R. L. Galvão[2]*, Rui Sun[1]*, Ralf I. Kaiser[1]*

Elementary reaction mechanisms constitute a fundamental infrastructure for chemical processes as a whole. However, while these mechanisms are well understood for second-period elements, involving those of the third period and beyond can introduce unorthodox reactivity. Combining crossed molecular beam experiments with electronic structure calculations and molecular dynamics simulations, we provide compelling evidence on an exotic insertion of an unsaturated sigma doublet radical into a silicon-hydrogen bond as observed in the barrierless gas-phase reaction of the D1-ethynyl radical (C_2D) with silane (SiH_4). This pathway, which leads to the D1-silylacetylene (SiH_3CCD) product via atomic hydrogen loss, challenges the prerequisite and fundamental concept that two reactive electrons and an empty orbital are required for the open shell, unsaturated radical reactant to insert into a single bond.

INTRODUCTION

Since the discovery of the very first organic free radical, triphenylmethyl [$^{\bullet}C(C_6H_5)_3$], by Gomberg in 1900 (*1*), crossed molecular beam experiments (*2*–*11*) advanced our fundamental understanding of the chemical dynamics of elementary reactions of prototype organic radicals such as methylidyne (CH, $X^2\Pi$) (*12*) and ethynyl (C_2H, $X^2\Sigma^+$) (*13*) involving abstraction [1], addition [2], and insertion [3] mechanisms on the molecular level (Fig. 1). The unique electronic structure of a doubly occupied, carbene-type *sp* orbital along with the singly occupied p_x and empty p_y orbitals of methylidyne (*14*) facilitates an abstraction of, e.g., atomic hydrogen (**1**), an addition pathway to, for instance, unsaturated carbon-carbon bonds (**2**), and an insertion into carbon-hydrogen single bonds (**3**). These pathways involve either direct reactions (abstraction) (*15*, *16*) or comprise indirect reaction dynamics through formation of reactive intermediates containing sp^2- and/or sp^3-hybridized carbon atoms. However, reactions of the ethynyl radical, where the radical center is essentially localized in the *sp* orbital (*17*), have been constrained only to hydrogen abstraction (**4**) and addition to unsaturated bonds of, e.g., olefins and acetylenes (**5**) (Fig. 1). The lack of an insertion pathway of the ethynyl radical into single bonds, e.g., carbon-hydrogen, has been attributed to the prerequisite that two electrons and an empty orbital (or an orbital that is easily emptied during interaction of the reactants) are required for the attacking reactant (X) so that two new single bonds (E—X and X—H) can be formed yielding the E—X—H moiety upon insertion into the single bond (E—H) of the other reactant (**6**) (*18*–*20*). These elementary gas-phase reactions signify vital prototypes that may proficiently increase the structural complexity of organic molecules often involving highly unsaturated, short-lived transient species such as homologous series of electron-deficient carbenes carrying divalent carbon atoms (*21*–*24*) with fundamental roles in preparative organic chemistry (*25*) and in chemical synthesis on the industrial scale (*26*).

Whereas the dynamics of these elementary reactions along with fundamental molecular mass growth processes up to, e.g., polycyclic aromatic hydrocarbons (*27*–*29*) through carbon-carbon bond coupling have been unraveled at the molecular level in impressive detail, the knowledge of abstraction [1], addition [2], and insertion [3] mechanisms involving closed-shell reactants carrying atoms of the third row, such as silicon, at the most fundamental, atomistic level has just scratched the surface. Recent crossed molecular beam studies of the gas-phase reactions of the cyano (CN, $X^2\Sigma^+$) (*30*) and phenyl (C_6H_5, X^2A_1) (*31*) radicals with silane (SiH_4) revealed, in addition to the expected hydrogen abstraction pathways (**7**) and (**8**), a facile radical substitution (S_R) mechanism via penta-coordinated silicon atoms involving Walden inversion (*32*) with a nearly collinear geometry of the attacking radical reactant and the leaving hydrogen [(**9**) and (**10**)]. Although these reactions have shaped our fundamental understanding in chemical synthesis (*33*) and in physical organic chemistry from the viewpoint of chemical bonding and molecular structure theory (*34*), especially for substituting functional groups (*35*) and facilitating carbon-silicon bond couplings (*36*, *37*), insertion pathways of ethynyl (C_2H, $X^2\Sigma^+$) radicals into single bonds carrying third row atoms such as the silicon-hydrogen moiety have been classified as "nonexistent" until now.

$^{\bullet}CN + SiH_4 \rightarrow HCN + {}^{\bullet}SiH_3$ (**7**)

$^{\bullet}C_6H_5 + SiH_4 \rightarrow C_6H_6 + {}^{\bullet}SiH_3$ (**8**)

$^{\bullet}CN + SiH_4 \rightarrow SiH_3CN + {}^{\bullet}H$ (**9**)

$^{\bullet}C_6H_5 + SiH_4 \rightarrow C_6H_5SiH_3 + {}^{\bullet}H$ (**10**)

Here, crossed molecular beam experiments of the D1-ethynyl radical (C_2D, $X^2\Sigma^+$) with silane (SiH_4, X^1A_1) merged with electronic structure calculations and quasi-classical trajectory (QCT) simulations grant a unique glance of the unconventional reaction dynamics in the gas-phase preparation of the D1-silylacetylene molecule (SiH_3CCD, X^1A_1) plus atomic hydrogen. Because the D1-ethynyl radical features no empty orbitals and silane is a closed-shell molecule with no double/triple bonds or electron lone pairs, only direct

[1]Department of Chemistry, University of Hawai'i at Mānoa, Honolulu, HI 96822, USA. [2]Centro Federal de Educação Tecnológica de Minas Gerais, Belo Horizonte 30421-169, Brazil.
*Corresponding author. Email: ralfk@hawaii.edu (R.I.K.); ruisun@hawaii.edu (R.S.); brenogalvao@gmail.com (B.R.L.G.)
†These authors contributed equally to this work.
‡Present address: Universidade Federal do Espírito Santo, Vitória 29075-910, Brazil.

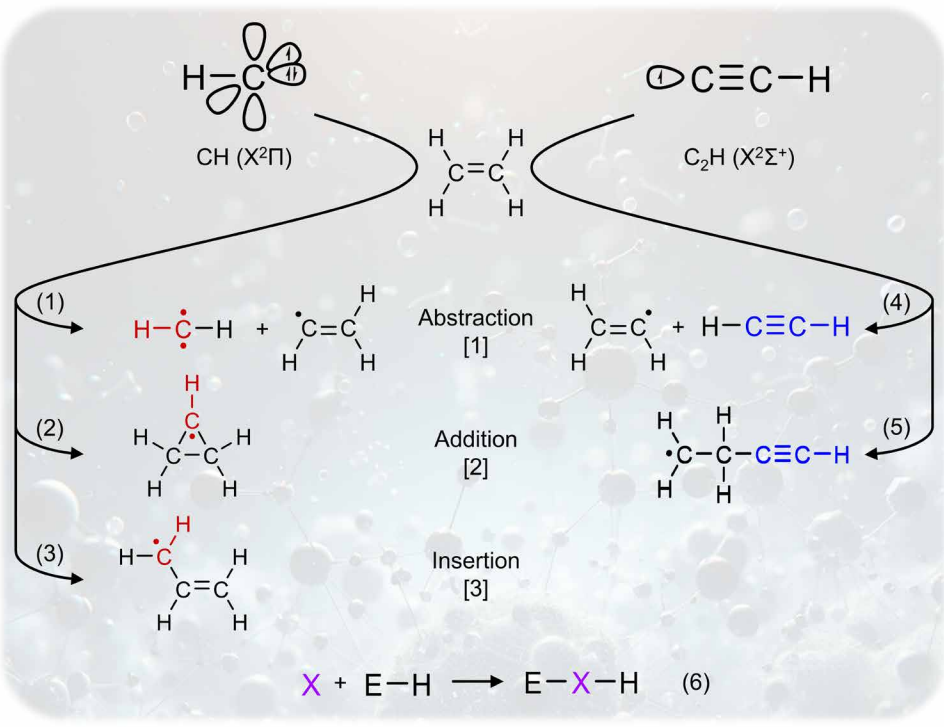

Fig. 1. Elementary reaction mechanisms. Schematic representation of the reactions of methylidyne (CH) and ethynyl (CCH) radicals with ethylene (C_2H_4) showcasing the abstraction [1], addition [2], and insertion [3] pathways, leading to products (reactions **1** and **4**) or the initial collision complex (reactions **2**, **3**, and **5**). The methylidyne moiety is highlighted in red and the ethynyl moiety is highlighted in blue. Reaction **6** refers to a general insertion mechanism.

reaction mechanisms are expected; however, as is detailed herein, this is unexpectedly not the case. The ethynyl-silane system can be classified as a prototype reaction with an unusual reactivity compared to the isovalent carbon system [methane (CH_4), X^1A_1], where only the hydrogen abstraction mechanism to D1-acetylene plus the methyl radical is open (*38*), exposing that isovalent systems such as C_2D-SiH_4 versus C_2D-CH_4 have distinct chemical reactivities. The combination of crossed molecular beam experiments with electronic structure calculations and QCT simulations as presented here affords fundamental reaction mechanisms and promotes intimate knowledge of bond-breaking and isomerization processes of highly reactive organometallic radical intermediates. The close match between experimental chemical dynamics studies and the conclusions from QCT simulations reveals that molecular beam studies merged with dynamics simulations have progressed to such a level that polyatomic reactions can be untangled at the molecular level, thus offering a unified picture of the underlying gas-phase chemistry and chemical bonding of isovalent systems involving silicon under single-collision conditions in the gas phase.

RESULTS

Laboratory reference frame

The bimolecular gas-phase reaction of D1-ethynyl radicals (C_2D, $X^2\Sigma^+$) with silane (SiH_4, X^1A_1) was conducted under single-collision conditions exploiting a crossed molecular beams machine (Materials and Methods). Time-of-flight (TOF) spectra were recorded at distinct mass/charge ratios (m/z) of 57 ($^{28}Si^{12}C_2H_3D^+$, $^{29}Si^{12}C_2H_2D^+$, $^{30}Si^{12}C_2H_3^+$, $^{30}Si^{12}C_2HD^+$, and $^{28}Si^{13}C^{12}CH_2D^+$), 56 ($^{28}Si^{12}C_2H_2D^+$, $^{28}Si^{12}C_2H_4^+$, $^{29}Si^{12}C_2HD^+$, $^{29}Si^{12}C_2H_3^+$, $^{30}Si^{12}C_2D^+$, $^{30}Si^{12}C_2H_2^+$, $^{28}Si^{13}C^{12}CHD^+$, and $^{28}Si^{13}C^{12}CH_3^+$), and 55 ($^{28}Si^{12}C_2HD^+$, $^{28}Si^{12}C_2H_3^+$, $^{29}Si^{12}C_2D^+$, $^{29}Si^{12}C_2H_2^+$, $^{30}Si^{12}C_2H^+$, $^{28}Si^{13}C^{12}CD^+$, and $^{28}Si^{13}C^{12}CH_2^+$). No signal was detected from m/z = 58 to 60, indicating that no adducts were produced. Accounting for the masses of the reactants of D1-ethynyl (26 u) and silane (28 u), signal at m/z = 57 can be associated with the formation of SiC_2H_3D (57 u) product(s) plus atomic hydrogen (1 u) (**11**). The TOFs at m/z = 57, 56, and 55 overlap after scaling (fig. S1), suggesting that signal at m/z = 56 and 55 originates from dissociative electron impact ionization of the parent product (SiC_2H_3D). Further, no deuterium atom loss was observed, revealing that the hydrogen atom ejection occurs from the silane reactant. Consequently, TOFs were acquired at m/z = 57 at the center-of-mass (CM) angle (Θ_{CM}) of 25.4° ± 0.9° as well as at higher and lower angles in 5° steps (Fig. 2B). All TOFs are broad, spanning ion counts about 400 to 800 μs. The corresponding laboratory angular distribution (LAD) was obtained by normalizing the angular TOFs to the CM angle (Fig. 2A). The LAD encompasses about 30° in the plane of the reactants and features a nearly forward-backward symmetry within the error limits. Overall, the laboratory data propose the D1-ethynyl versus atomic hydrogen exchange on the silane moiety (**11**) forming SiC_2H_3D isomer(s) in the gas phase.

$$^{\bullet}C_2D\ (26\ u) + SiH_4\ (32\ u) \rightarrow SiC_2H_3D\ (57\ u) + {}^{\bullet}H\ (1\ u)\ (\mathbf{11})$$

CM reference frame

With the detection of SiC_2H_3D product(s), we now extract information on the reaction dynamics along with the nature of the intermediates and products. This is accomplished through a transformation of the data from the laboratory reference frame to the CM reference

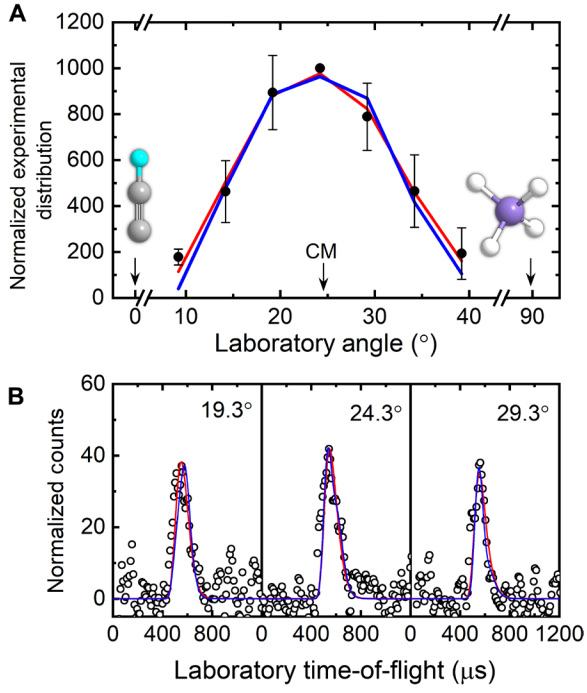

Fig. 2. Data in the laboratory reference frame. Laboratory angular distribution (LAD) (**A**) and time-of-flight (TOF) spectra (**B**) recorded at mass/charge ratio (*m*/*z*) = 57 for the reaction of the D1-ethynyl radical (C_2D) with silane (SiH_4). CM represents the center-of-mass angle, and 0° and 90° define the directions of the D1-ethynyl and silane beams, respectively. The black circles depict the data, red lines depict the experimental fits, and blue lines depict the dynamics simulations fits. Carbon atoms are colored gray, silicon is purple, hydrogen is white, and deuterium is light blue.

frame (Materials and Methods), yielding the CM translational energy [$P(E_T)$] and angular [$T(\theta)$] flux distributions together with the associated flux contour map (Fig. 3). The $P(E_T)$ (Fig. 3A) can be used to extract the reaction energy ($\Delta_r G$) accounting for energy conservation ($\Delta_r G = E_C - E_{max}$) (*39*) for those products formed without internal excitation with the collision energy E_C and the maximum product translational energy E_{max}. The $P(E_T)$ exhibits an E_{max} of 204 ± 31 kJ mol^{-1}, which results in a reaction energy of 164 ± 32 kJ mol^{-1} at the experimental collision energy of 40.2 ± 1.3 kJ mol^{-1}. In addition, the $P(E_T)$ peaks in the vicinity of 45 kJ mol^{-1}, which is indicative of a tight exit transition state to the product(s). The flux contour map $T(\theta)$ (Fig. 3B) features a forward-backward symmetry and intensity over the complete angular range suggestive of indirect reactive scattering dynamics through complex formation (SiC_2H_4D) (*39*) whose lifetime is longer than its rotation period. The weak polarization of the $T(\theta)$ is the direct result of the inability of the light hydrogen atom to carry away a substantial fraction of the total angular momentum, which, in turn, leads to a substantial rotational excitation of the final products. These findings are reflected in the flux contour map (Fig. 3C).

Potential energy surface

Electronic structure calculations were conducted at the CCSD(T)-F12/cc-pVTZ-F12//B2PLYP-D3/cc-pV(T+d)Z + ZPE(B2PLYP-D3/cc-pV(T+d)Z) level of theory to provide energies of the reactants, transition states, and products with an expected accuracy of ±4 kJ mol^{-1} (*40*). These calculations identified product channels, leading to the D1-silylacetylene molecule (SiH_3CCD, X^1A_1, **p1**) plus atomic hydrogen and also to the silyl radical (SiH_3, X^2A_1, **p2**) plus D1-acetylene (C_2HD, $X^1\Sigma^+$) (Fig. 4). The computationally predicted exoergicity of the reaction of −151 ± 4 kJ mol^{-1} to prepare the D1-silylacetylene molecule correlates nicely with the experimentally derived reaction energy of −164 ± 32 kJ mol^{-1}, thus providing compelling evidence on the gas-phase preparation of C_{3v} symmetric D1-silylacetylene via the elementary reaction of the D1-ethynyl radical with silane (**11**). In detail, our computations identify three reaction pathways to D1-silylacetylene involving direct and indirect (complex forming) dynamics. First, extensive geometry scans near the configurational space connecting the separated reactants to the final products D1-silylacetylene plus atomic hydrogen show that the potential energy monotonically decreases. This pathway implicates a radical substitution mechanism (S_R) (*41*), in which the silicon atom is pentacoordinated depicting a trigonal bipyramidal geometry (structure shown in Fig. 5A), where the D1-ethynyl radical is present at one of the apices. This is reflected in a nearly collinear (180°) geometry of the axial Si—H bond with the D1-ethynyl moiety along with a simultaneous bond-forming–bond-breaking process and Walden inversion of the hydrogen atoms at the silicon atom.

Besides radical substitution (S_R), two additional mechanisms involve indirect scattering dynamics through complex formation (SiC_2H_4D). In the minimum energy path associated with the approach of the two reactants, the D1-ethynyl radical performs an unusual insertion into one of the Si—H bonds of silane, which occurs without any activation energy. This leads to the doublet radical intermediate **i1** (X^2A'), which resides in a deep potential energy well and is stabilized by 266 kJ mol^{-1} with respect to the separated reactants. The 2-silylethenyl intermediate **i1** either undergoes unimolecular decomposition via atomic hydrogen loss through a tight exit transition state located 21 kJ mol^{-1} above the energy of the separate products, forming D1-silylacetylene (**p1**), or isomerizes via atomic hydrogen shift, yielding intermediate **i2** (X^2A') before its fragmentation to **p1** through hydrogen loss. The hydrogen shift (**i1** → **i2**) is associated with a barrier of 164 kJ mol^{-1} but resides well below the energy of the separated reactants and, hence, can be crossed easily. Overall, the electronic structure calculations predict up to three energetically accessible channels to the observed D1-silylacetylene molecule involving direct and indirect (**i1** → **p1** + H; **i1** → **i2** → **p1** + H) scattering dynamics. However, which of the three pathways truly leads to the formation of D1-silylacetylene?

Molecular dynamics simulations

This open query commands QCT calculations, thus bridging the dynamics experiments with the theoretical understanding of the D1-ethynyl–silane system. These trajectory studies reveal exciting results and provide compelling evidence confirming the three reaction mechanisms (see the previous section), leading to the gas-phase formation of the experimentally observed D1-silylacetylene molecule (SiH_3CCD, **p1**). Of the 1000 reactive trajectories, about 25% led to the formation of **p1**; an account of the remaining trajectories can be found in Materials and Methods. Because of excess energy in the system, the trajectories do not experience the exact structures reported in Fig. 4, and snapshots of one example trajectory of each mechanism are depicted in Fig. 5. About 34% of the **p1**-forming trajectories follow direct scattering dynamics via a radical substitution mechanism (S_R) (Fig. 5A), with a further breakdown depicted in

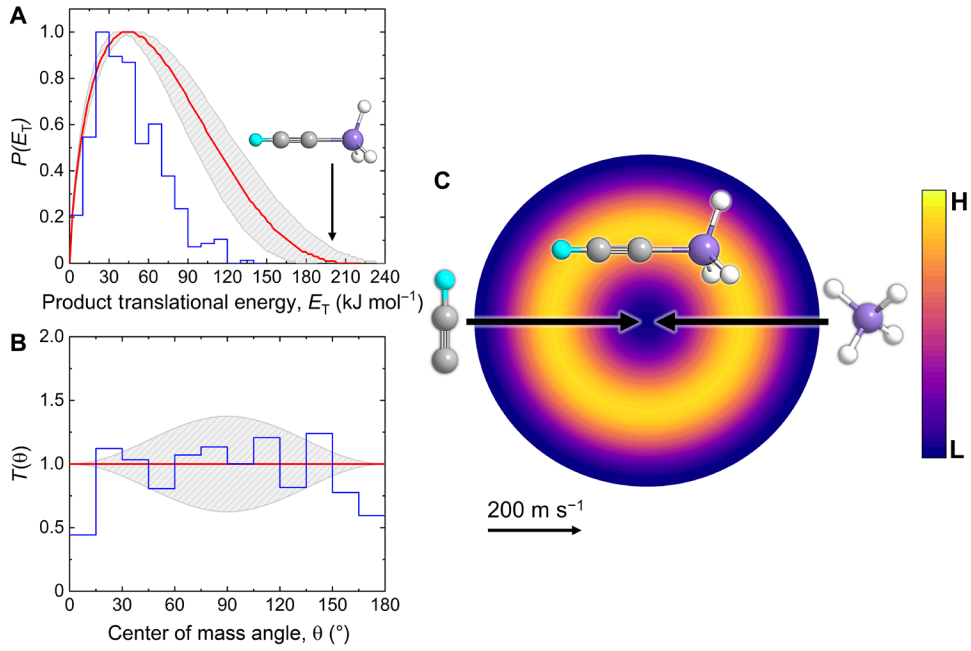

Fig. 3. Data in the CM reference frame. CM product translational energy (**A**) and angular (**B**) flux distributions, as well as the associated flux contour map (**C**), leading to the formation of SiC_2H_3D isomer(s) in the reaction of D1-ethynyl (C_2D) with silane (SiH_4). Red lines define the best-fit functions, while shaded areas provide the error limits. The CM functions overlaid in blue are obtained from the dynamics simulations. The flux contour map represents the intensity of the reactively scattered products as a function of product velocity (*u*) and scattering angle (θ), and the color bar indicates flux gradient from high (H) to low (L) intensity.

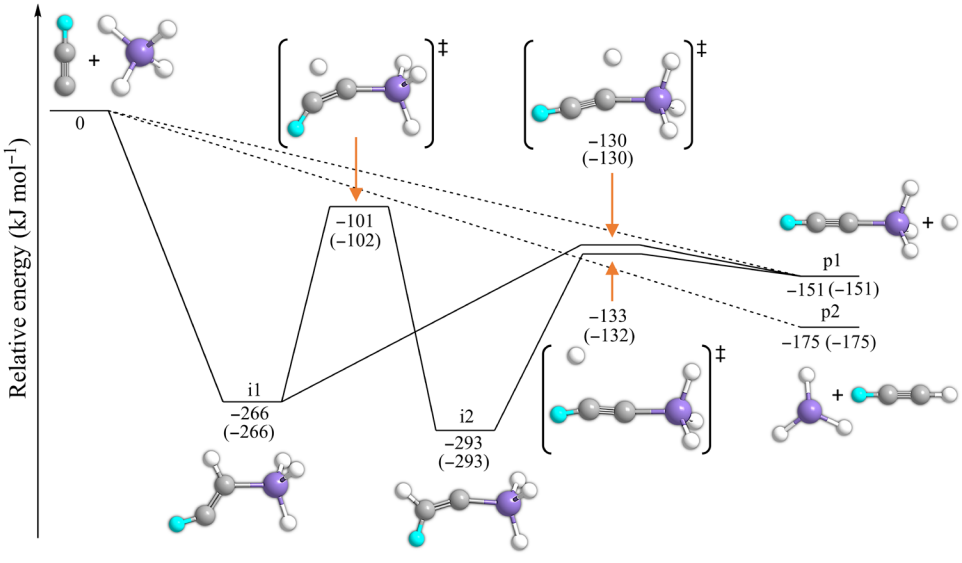

Fig. 4. Simplified potential energy surface of the $C_2D + SiH_4$ reaction. Schematic potential energy surface for the reaction of the D1-ethynyl radical (C_2D) with silane (SiH_4), leading to **p1** and **p2** at the CCSD(T)-F12/cc-pVTZ-F12//B2PLYP-D3/cc-pV(T+d)Z + ZPE(B2PLYP-D3/cc-pV(T+d)Z) level. Energies for the ethynyl (C_2H)–silane (SiH_4) system are given in parenthesis, and dotted lines denote direct reaction mechanisms.

fig. S3. As the D1-ethynyl radical approaches silane with its unpaired electron in the collinear sigma orbital, the hydrogen atoms undergo Walden inversion while one of the silicon-hydrogen bonds elongate, culminating in the eventual emission of the hydrogen atom and silicon-carbon bond formation in D1-silylacetylene.

The dominating fraction (66%) of the **p1**-forming trajectories follow indirect scattering dynamics through an unconventional insertion pathway via 2-silylethenyl (**i1**). The D1-ethynyl radical approaches silane in a sideway orientation instead of collinearly as in the substitution case (Fig. 5B). With hydrogen being transferred from silicon to carbon, the reaction path leads energetically downhill via efficient insertion of the D1-ethynyl radical into the silicon-hydrogen bond to intermediate **i1**, which ejects a hydrogen atom forming the separated products. The QCT simulations identify a

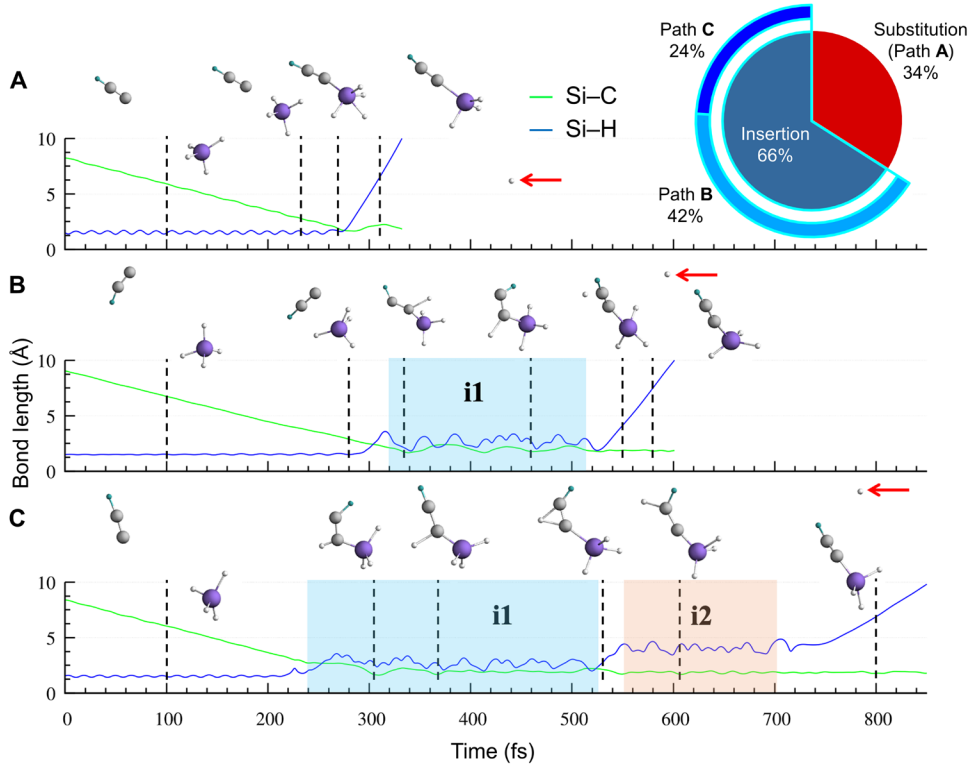

Fig. 5. Representative trajectories for the substitution and insertion mechanisms. Key distances of the carbon-silicon (green line) and silicon–leaving-hydrogen-atom (blue line) versus time for the substitution (**A**) and insertion (**B** and **C**) reaction mechanisms with snapshots inserted from representative trajectories. The ejected hydrogen atom is highlighted with a red arrow in the final snapshot. The pie chart represents the percentage of reactive trajectories which follow substitution (red area) and insertion (blue area).

second route from **i1** (Fig. 5C). Rather than undergoing carbon-hydrogen bond cleavage as in the previous case, a hydrogen shift to the terminal carbon atom yields **i2** featuring a D1-methylene moiety. Similar hydrogen migration reactions along unsaturated carbon chains with comparable accessible energy have been reported previously (*42*, *43*). This intermediate then ejects atomic hydrogen, ultimately generating D1-silylacetylene. It is worth noting that the dynamics simulations did identify not only an atomic hydrogen loss from **i2** but also an atomic deuterium loss (65% H loss and 35% D loss). Considering that 34% of the reactive trajectories leading to D1-silylacetylene are direct, 42% of the trajectories follow the **i1** → **p1** + H mechanism, and only 24% involve yet the second intermediate via **i1** → **i2** → **p1** + H, the overall hydrogen to deuterium branching ratio is predicted to be 92% versus 8%. The low predicted fraction of the emitted deuterium might explain its experimental non-detection. We would like to note that although the electronic structure calculations also revealed pathways to higher energy isomers of **p1** (fig. S2), the dynamics simulations suggest that these high energy isomers are not formed in the gas-phase reaction of D1-ethynyl with silane.

To gauge the predictive power and, hence, the quality of the QCT simulations, the theoretically derived CM translational energy and scattering angle distributions are compared with the experimental TOF and LAD data (Figs. 2 and 3). Considering the CM angular distribution, the dynamics simulations predict an essentially forward-backward symmetric distribution with fluxes in the vicinity of the poles substantially lower compared to the broad, nearly isotropic plateau from 20° to 150°. Within the error limits, the predicted CM angular distribution agrees well with the experiments. The translational energy distribution also forecasts a broad distribution maximum from 30 to 60 kJ mol^{-1}, which correlates well with the maximum of the simulated translational energy distribution of 45 kJ mol^{-1}. The highest CM translational energy found in the QCT simulations is 150 kJ mol^{-1}, smaller than the experimental findings of 205 ± 25 kJ mol^{-1}. Nevertheless, the CM functions obtained from the dynamics simulations replicate the TOF data and the LAD exceptionally well (Fig. 2), disclosing that dynamics calculations of complex systems such as for the D1-ethynyl–silane system have advanced to such a level to forecast the chemical dynamics of complex, multiatomic systems including "heavy" reactants with elements of the third row quantitatively.

DISCUSSION

An unconventional insertion by an unsaturated doublet hydrocarbon radical was discovered in the bimolecular gas-phase reaction of the D1-ethynyl radical (C_2D) with silane (SiH_4) as explored under single-collision conditions by the crossed molecular beam technique coupled with electronic structure calculations and molecular dynamics simulations. The reaction pathways lead via atomic hydrogen loss to the D1-silylacetylene molecule (SiH_3CCD) through carbon-silicon bond coupling as observed experimentally featuring both direct and indirect entrance channels, in which one-third of the reactive trajectories access a radical substitution (S_R) pathway

without barrier through D1-ethynyl radical center attack on the silane silicon atom and simultaneous hydrogen ejection and Walden inversion. The remaining two-thirds follow a unique barrierless insertion of the terminal D1-ethynyl carbon into a Si—H bond of silane, where the 2-silylethenyl intermediate undergoes either unimolecular decomposition via atomic hydrogen loss or a [1,2]-H shift before ejection of a hydrogen atom preparing D1-silylacetylene in overall exoergic reactions. The D1-ethynyl radical reactivity with silane can be compared to the isovalent carbon-centered counterpart methane (CH_4). In the ethynyl–methane system, the abstraction pathway leading over an 11 kJ mol^{-1} barrier to the methyl radical (CH_3) plus acetylene (C_2H_2) is the most energetically favored pathway, while radical substitution to methylacetylene (CH_3CCH) via atomic hydrogen loss features a high barrier of 72 kJ mol^{-1} (*38*). Both mechanisms require substantial input energy (e.g., high temperatures) to overcome the barriers to reaction, while the barrierless nature of the equivalent routes in the C_2H-SiH_4 system allows rapid access at low temperatures. The pathway in the reaction of ethynyl with methane featuring insertion of the terminal ethynyl carbon into a carbon-hydrogen bond of methane, in analogy to the insertion mechanism observed in the current study, was not found. The large difference in the reactivity of methane and silane with respect to collisions with the ethynyl radical can be rationalized from the difference in their frontier orbitals (Fig. 6). While methane has a nondegenerate lowest unoccupied molecular orbital (LUMO) (more localized in the hydrogen atoms), silane presents three degenerate unoccupied orbitals that are substantially different from that of methane. The percentage contributions per basis function type on each atom were assessed by evaluating the Löwdin reduced orbital population, which proves that a strong *d* character could be observed in all three degenerate LUMOs of silane, while no *d*-orbital contribution is present in the frontier molecular orbitals of methane. Overall, the ethynyl-silane reaction represents a fundamental framework showcasing the unique dynamics of isovalent systems, i.e., C_2D-SiH_4 versus C_2D-CH_4, in main group XIV, furthering our knowledge of similarities and differences of the chemical bonding and reactivity of isovalent systems at their roots.

MATERIALS AND METHODS

Experimental methods

The reactions of the D1-ethynyl radical (C_2D, $X^2\Sigma^+$) with silane (SiH_4, 99.999%, Linde) were conducted under single-collision conditions using a crossed molecular beams machine (*44*). Briefly, a pulsed supersonic D1-ethynyl beam was produced in situ via laser ablation of a rotating graphite rod using the fourth harmonic of a Nd:YAG laser (Quanta-Ray Pro 270, Spectra-Physics) at 30 Hz and 7 to 10 mJ per pulse. The ablated species were seeded in neat deuterium gas (D_2, 99.999%, Linde) at a backing pressure of 3000 torr, which also acted as a reactant, where atomic deuterium abstraction by dicarbon (C_2) yields the D1-ethynyl radical (*45*–*47*). The reactant beam was skimmed then velocity selected by a four-slot chopper wheel, giving peak velocities (v_p) of 2218 ± 34 m s^{-1} and speed ratios (S) of 4.4 ± 0.4. Any D1-ethynyl radicals formed in the $A^2\Pi$ excited state, which has a lifetime of <1 μs, relaxed back to the $X^2\Sigma^+$ ground state in the ~30-μs time interval for the radical to travel from the ablation center to the interaction region (*48*). The D1-ethynyl beam crossed perpendicularly with a neat silane beam (SiH_4, v_p = 827 ± 20 m s^{-1}, S = 10.1 ± 0.2) pulsed at 60 Hz and −400 V with a backing pressure of 550 torr, granting a collision energy (E_c) of 40.2 ± 1.3 kJ mol^{-1} and CM angle (Θ_{CM}) of 25.4 ± 0.9°. It should be noted that the laser ablation also produces carbon atoms, as well as dicarbon and tricarbon molecules. Carbon and dicarbon have masses 14 and 2 u less than the D1-ethynyl radical, respectively, and thus do not interfere with observed signal in the present study. Assuming the possibility of reactions of tricarbon with silane, this would produce a C_3SiH_4 collision complex at

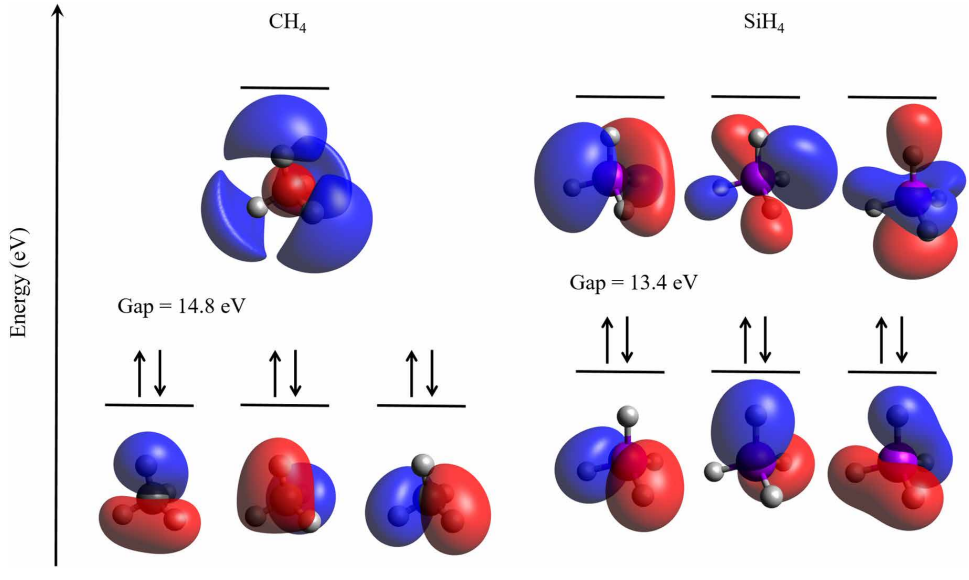

Fig. 6. Frontier orbitals for methane and silane. Comparison between the lowest unoccupied molecular orbitals (LUMOs) of the isovalent methane and silane molecules. Methane features a nondegenerate LUMO strongly localized in the hydrogen atoms, while those of silane are triply degenerate with strong *d* character and a smaller highest occupied molecular orbital–LUMO gap.

$m/z = 68$; however, there are no possible fragments that can give signal at the $m/z = 57$ observed for the title reaction.

Reactively scattered products were collected by a triply differentially pumped mass spectrometric detector that is rotatable in the plane defined by both reactant beams. Products are ionized by electron impact ionization at 80 eV and emission current of 2 mA before mass filtering via a quadrupole mass spectrometer (150QC, Extrel) operating in the TOF mode. Up to 7.2×10^6 TOF spectra were collected at each angle in 5° steps for the range $10° \leq \Theta \leq 40°$ with respect to the D1-ethynyl beam ($\Theta = 0°$). Integrating the TOFs and normalizing to the CM angle created a LAD. To obtain information on the chemical dynamics, the laboratory data were fit using a forward convolution routine, in which user-defined CM translational energy [$P(E_T)$] and angular [$T(\theta)$] flux distributions were refined iteratively until a reasonable fit of the data was achieved (*49*, *50*). The image of the overall outcome of the reaction was developed from these functions, defined as $I(u,\theta) \approx P(u) \times T(\theta)$, and is portrayed as a flux contour map (*4*).

Electronic structure calculations

The potential energy surface for the reaction of D1-ethynyl (C_2D) with silane (SiH_4) was obtained by quantum chemical calculations using the MOLPRO (*51*) and ORCA (*52*, *53*) software. First, geometry optimizations were carried out at the density functional theory (*54*) level using the B2PLYP-D3 double hybrid functional including Grimme's dispersion correction and Becke-Johnson damping (*55*, *56*) coupled with the cc-pV(T+d)Z basis set (*57*–*59*). At each stationary structure obtained, a harmonic vibrational analysis was performed at the same level of theory to extract vibrational frequencies and zero-point energy (ZPE) corrections. In the case of transition state structures, their connections to other structures were confirmed by performing intrinsic reaction coordinate calculations. Even though the final coordinates and frequencies are at the B2PLYP-D3/cc-pV(T+d)Z level, the energies were subsequently refined by performing single point calculations using the explicitly correlated RCCSD(T)-F12 (*60*, *61*) method with the cc-pVTZ-F12 basis set (*62*). This calculation strategy is hereafter denoted as CCSD(T)-F12/cc-pVTZ-F12//B2PLYP-D3/cc-pV(T+d)Z + ZPE(B2PLYP-D3/cc-pV(T+d)Z) with refined energies providing accuracies within 4 kJ mol^{-1} (*40*).

Ab initio molecular dynamics simulations

The ab initio molecular dynamics simulations were performed with a combined software package of NWChem (*63*) and VENUS (*64*, *65*), where the energy gradients calculated using NWChem were passed on to VENUS to solve the classical equations of motion to propagate the trajectories. The reactants, C_2D and SiH_4, were initially separated by 9 Å. To match conditions of the experiment, the rotational and vibrational energies of each reactant were sampled corresponding to a fixed temperature of 10 K. Velocity verlet (*66*, *67*) with a time step of 0.1 fs was used to propagate the trajectories, and, for those trajectories that have an energy jump of 1 kcal mol^{-1} or larger, the time step was reduced and restarted with the same initial conditions. The trajectories were stopped once the products or the reactants were 12 Å apart. The reactants collided with each other with a fixed translational energy of 40.2 kJ mol^{-1} at fixed impact parameters (b) between 0 and b_{max}, where b_{max} is the maximum b at which none of the collisions result in products. b_{max}, which was 5.0 Å in this study, was determined by sampling 50 trajectories at each b starting from 0 to 6.0 Å with a stride of $\Delta b = 0.5$ Å. Once b_{max} was determined, fixed b values were sampled from 0 to 5 Å with $\Delta b = 0.25$ Å and at each b, 120 trajectories were sampled, resulting in a grand total of 2520 trajectories. To account for the collision probability that is directly proportional to b (*68*), the scattering angle, product translational energy distributions, and percent branching ratios of the products were weighted by b.

Supplementary Materials

The PDF file includes:

Supplementary Text
Figs. S1 to S3
Table S1
Data S1
Legend for data S2
References

Other Supplementary Material for this manuscript includes the following:

Data S2

REFERENCES AND NOTES

1. M. Gomberg, An instance of trivalent carbon: Triphenylmethyl. *J. Am. Chem. Soc.* **22**, 757–771 (1900).
2. Y. T. Lee, Molecular beam studies of elementary chemical processes. *Science* **236**, 793–798 (1987).
3. H. Pan, K. Liu, A. Caracciolo, P. Casavecchia, Crossed beam polyatomic reaction dynamics: Recent advances and new insights. *Chem. Soc. Rev.* **46**, 7517–7547 (2017).
4. R. I. Kaiser, Experimental investigation on the formation of carbon-bearing molecules in the interstellar medium via neutral−neutral reactions. *Chem. Rev.* **102**, 1309–1358 (2002).
5. H. Li, A. G. Suits, Universal crossed beam imaging studies of polyatomic reaction dynamics. *Phys. Chem. Chem. Phys.* **22**, 11126–11138 (2020).
6. X. Yang, State-to-state dynamics of elementary bimolecular reactions. *Annu. Rev. Phys. Chem.* **58**, 433–459 (2007).
7. D. R. Albert, H. F. Davis, Studies of bimolecular reaction dynamics using pulsed high-intensity vacuum-ultraviolet lasers for photoionization detection. *Phys. Chem. Chem. Phys.* **15**, 14566–14580 (2013).
8. F. Fernández-Alonso, R. N. Zare, Scattering resonances in the simplest chemical reaction. *Annu. Rev. Phys. Chem.* **53**, 67–99 (2002).
9. M. Costes, C. Naulin, Observation of quantum dynamical resonances in near cold inelastic collisions of astrophysical molecules. *Chem. Sci.* **7**, 2462–2469 (2016).
10. K. Liu, Perspective: Vibrational-induced steric effects in bimolecular reactions. *J. Chem. Phys.* **142**, 080901 (2015).
11. J. J. Lin, Dynamics of reactions between two closed-shell molecules. *Phys. Chem. Chem. Phys.* **13**, 19206–19213 (2011).
12. F. Zhang, P. Maksyutenko, R. I. Kaiser, Chemical dynamics of the $CH(X^2\Pi) + C_2H_4(X^1A_{1g})$, $CH(X^2\Pi) + C_2D_4(X^1A_{1g})$, and $CD(X^2\Pi) + C_2H_4(X^1A_{1g})$ reactions studied under single collision conditions. *Phys. Chem. Chem. Phys.* **14**, 529–537 (2012).
13. F. Zhang, Y. S. Kim, R. I. Kaiser, S. P. Krishtal, A. M. Mebel, Crossed molecular beams study on the formation of vinylacetylene in Titan's atmosphere. *J. Phys. Chem. A* **113**, 11167–11173 (2009).
14. P. F. Bernath, C. R. Brazier, T. Olsen, R. Hailey, W. T. M. L. Fernando, C. Woods, J. L. Hardwick, Spectroscopy of the CH free radical. *J. Mol. Spectrosc.* **147**, 16–26 (1991).
15. R. D. Levine, R. B. Bernstein, *Molecular Reaction Dynamics and Chemical Reactivity* (Oxford Univ. Press, 1987).
16. M. Brouard, C. Vallance, *Tutorials in Molecular Reaction Dynamics*, M. Brouard, C. Vallance, Eds. (The Royal Society of Chemistry, 2010).
17. P. G. Carrick, A. J. Merer, R. F. Curl Jr., $\tilde{A}^2\Pi \leftarrow \tilde{X}^2\Sigma^+$ infrared electronic transition of C_2H. *J. Chem. Phys.* **78**, 3652–3658 (1983).
18. P. Sykes, *A Guidebook to Mechanism in Organic Chemistry* (Longman Scientific & Technical, 1986).
19. H. Kollmar, Insertion reaction of a nucleophilic carbene. A molecular orbital theoretical study. *J. Am. Chem. Soc.* **100**, 2660–2664 (1978).
20. Z.-X. Wang, M.-B. Huang, R.-Z., Liu, Theoretical study on the insertion reaction of $CH(X^2\Pi)$ with CH_4. *Can. J. Chem.* **75**, 996–1001 (1997).
21. R. A. Seburg, R. J. McMahon, Automerizations and isomerizations in propynylidene (HCCCH), propadienylidene (H_2CCC), and cyclopropenylidene (c-C_3H_2). *Angew. Chem. Int. Ed.* **34**, 2009–2012 (1995).
22. R. A. Seburg, J. T. DePinto, E. V. Patterson, R. J. McMahon, Structure of triplet propynylidene. *J. Am. Chem. Soc.* **117**, 835–836 (1995).

23. R. A. Seburg, E. V. Patterson, J. F. Stanton, R. J. McMahon, Structures, automerizations, and isomerizations of C_3H_2 isomers. *J. Am. Chem. Soc.* **119**, 5847–5856 (1997).
24. R. A. Seburg, R. J. McMahon, J. F. Stanton, J. Gauss, Structures and stabilities of C_5H_2 isomers: Quantum chemical studies. *J. Am. Chem. Soc.* **119**, 10838–10845 (1997).
25. Z.-Y. Xie, J. Xuan, Advances in heterocycle synthesis through photochemical carbene transfer reactions. *Chem. Commun.* **60**, 2125–2136 (2024).
26. J. C. Mol, Industrial applications of olefin metathesis. *J. Mol. Catal. A Chem.* **213**, 39–45 (2004).
27. R. I. Kaiser, N. Hansen, An aromatic universe – A physical chemistry perspective. *J. Phys. Chem. A* **125**, 3826–3840 (2021).
28. E. Reizer, B. Viskolcz, B. Fiser, Formation and growth mechanisms of polycyclic aromatic hydrocarbons: A mini-review. *Chemosphere* **291**, 132793 (2022).
29. H. Richter, J. B. Howard, Formation of polycyclic aromatic hydrocarbons and their growth to soot—A review of chemical reaction pathways. *Prog. Energy Combust. Sci.* **26**, 565–608 (2000).
30. Z. Yang, C. He, S. J. Goettl, D. Paul, R. I. Kaiser, M. X. Silva, B. R. L. Galvão, Gas-phase preparation of silyl cyanide (SiH_3CN) via a radical substitution mechanism. *J. Am. Chem. Soc.* **144**, 8649–8657 (2022).
31. M. Lucas, A. M. Thomas, T. Yang, R. I. Kaiser, A. M. Mebel, D. Hait, M. Head-Gordon, Bimolecular reaction dynamics in the phenyl–silane system: Exploring the prototype of a radical substitution mechanism. *J. Phys. Chem. Lett.* **9**, 5135–5142 (2018).
32. P. Walden, Ueber die gegenseitige umwandlung optischer antipoden. *Ber. Dtsch. Chem. Ges.* **29**, 133–138 (1896).
33. C. H. Schiesser, L. M. Wild, Free-radical homolytic substitution: New methods for formation of bonds to heteroatoms. *Tetrahedron* **52**, 13265–13314 (1996).
34. A. Ayasli, A. Khan, T. Michaelsen, T. Gstir, M. Ončák, R. Wester, Imaging frontside and backside attack in radical ion–molecule reactive scattering. *J. Phys. Chem. A* **127**, 5565–5571 (2023).
35. X. Wu, C. Zhu, Radical-mediated remote functional group migration. *Acc. Chem. Res.* **53**, 1620–1636 (2020).
36. J.-S. Li, J. Wu, Recent developments in the photo-mediated generation of silyl radicals and their application in organic synthesis. *ChemPhotoChem* **2**, 839–846 (2018).
37. S. Bähr, W. Xue, M. Oestreich, C(sp3)–Si cross-coupling. *ACS Catal.* **9**, 16–24 (2019).
38. B. Ceursters, H. M. Thi Nguyen, J. Peeters, M. Tho Nguyen, Experimental and theoretical study of the gas phase reaction of ethynyl radical with methane ($HC{\equiv}C+CH_4$). *Chem. Phys. Lett.* **329**, 412–420 (2000).
39. W. B. Miller, S. A. Safron, D. R. Herschbach, Exchange reactions of alkali atoms with alkali halides: A collision complex mechanism. *Discuss. Faraday Soc.* **44**, 108 (1967).
40. J. Zhang, E. F. Valeev, Prediction of reaction barriers and thermochemical properties with explicitly correlated coupled-cluster methods: A basis set assessment. *J. Chem. Theory Comput.* **8**, 3175–3186 (2012).
41. M. B. Smith, J. March, *March's Advanced Organic Chemistry: Reactions, Mechanisms, and Structure* (John Wiley & Sons, 2006).
42. C. He, Z. Yang, S. Doddipatla, A. M. Thomas, R. I. Kaiser, G. R. Galimova, A. M. Mebel, K. Fujioka, R. Sun, Directed gas phase preparation of ethynylallene ($H_2CCCHCCH$; X^1A') via the crossed molecular beam reaction of the methylidyne radical (CH; $X^2\Pi$) with vinylacetylene ($H_2CCHCCH$; X^1A'). *Phys. Chem. Chem. Phys.* **24**, 26499–26510 (2022).
43. C. He, K. Fujioka, A. A. Nikolayev, L. Zhao, S. Doddipatla, V. N. Azyazov, A. M. Mebel, R. Sun, R. I. Kaiser, A chemical dynamics study of the reaction of the methylidyne radical (CH, $X^2\Pi$) with dimethylacetylene (CH_3CCCH_3, X^1A_{1g}). *Phys. Chem. Chem. Phys.* **24**, 578–593 (2021).
44. X. Gu, Y. Guo, R. I. Kaiser, Mass spectrum of the butadiynyl radical (C_4H; $X^2\Sigma^+$). *Int. J. Mass Spectrom.* **246**, 29–34 (2005).
45. F. Zhang, D. Parker, Y. S. Kim, R. I. Kaiser, A. M. Mebel, On the formation of ortho-benzyne ($o\text{-}C_6H_4$) under single collision conditions and its role in interstellar chemistry. *Astrophys. J.* **728**, 141 (2011).
46. B. M. Jones, F. Zhang, R. I. Kaiser, A. Jamal, A. M. Mebel, M. A. Cordiner, S. B. Charnley, Formation of benzene in the interstellar medium. *Proc. Natl. Acad. Sci. U.S.A.* **108**, 452–457 (2011).
47. B. B. Dangi, D. S. N. Parker, R. I. Kaiser, A. Jamal, A. M. Mebel, A combined experimental and theoretical study on the gas-phase synthesis of toluene under single collision conditions. *Angew. Chem. Int. Ed.* **52**, 7186–7189 (2013).
48. S. J. Goettl, C. He, D. Paul, A. A. Nikolayev, V. N. Azyazov, A. M. Mebel, R. I. Kaiser, Gas-phase study of the elementary reaction of the D1-ethynyl radical (C_2D; $X^2\Sigma^+$) with propylene (C_3H_6; X^1A') under single-collision conditions. *J. Phys. Chem. A* **126**, 1889–1898 (2022).
49. M. F. Vernon, thesis, University of California at Berkeley (1983).
50. P. S. Weiss, thesis, University of California at Berkeley (1985).
51. H. J. Werner, P. J. Knowles, G. Knizia, F. R. Manby, M. Schütz, P. Celani, W. Györffy, D. Kats, T. Korona, R. Lindh, A. Mitrushenkov, G. Rauhut, K. R. Shamasundar, T. B. Adler, R. D. Amos, A. Bernhardsson, A. Berning, D. L. Cooper, J. O. Deegan, A. J. Dobbyn, F. Eckert, E. Goll, C. Hampel, A. Hesselmann, G. Hetzer, T. Hrenar, G. Jansen, C. Köppl, Y. Liu, A. W. Lloyd, R. A. Mata, A. J. May, S. J. McNicholas, W. Meyer, M. E. Mura, A. Nicklass, D. P. O'Neill, P. Palmieri, D. Peng, K. Pflüger, R. Pitzer, M. Reiher, T. Shiozaki, H. Stoll, A. J. Stone, R. Tarroni, T. Thorsteinsson, M. Wang, MOLPRO, a package of ab initio programs, version 2015.1 (University of Cardiff, Cardiff, UK, 2015); www.molpro.net.
52. F. Neese, The ORCA program system. *WIREs Comput. Mol. Sci.* **2**, 73–78 (2012).
53. F. Neese, Software update: The ORCA program system, version 4.0. *WIREs Comput. Mol. Sci.* **8**, e1327 (2018).
54. W. Kohn, L. J. Sham, Self-consistent equations including exchange and correlation effects. *Phys. Rev.* **140**, A1133–A1138 (1965).
55. S. Grimme, Semiempirical hybrid density functional with perturbative second-order correlation. *J. Chem. Phys.* **124**, 034108 (2006).
56. S. Grimme, J. Antony, S. Ehrlich, H. Krieg, A consistent and accurate ab initio parametrization of density functional dispersion correction (DFT-D) for the 94 elements H-Pu. *J. Chem. Phys.* **132**, 154104 (2010).
57. T. H. Dunning Jr., Gaussian basis sets for use in correlated molecular calculations. I. The atoms boron through neon and hydrogen. *J. Chem. Phys.* **90**, 1007–1023 (1989).
58. T. H. Dunning Jr., K. A. Peterson, A. K. Wilson, Gaussian basis sets for use in correlated molecular calculations. X. The atoms aluminum through argon revisited. *J. Chem. Phys.* **114**, 9244–9253 (2001).
59. R. A. Kendall, T. H. Dunning Jr., R. J. Harrison, Electron affinities of the first-row atoms revisited. Systematic basis sets and wave functions. *J. Chem. Phys.* **96**, 6796–6806 (1992).
60. T. B. Adler, G. Knizia, H.-J. Werner, A simple and efficient CCSD (T)-F12 approximation. *J. Chem. Phys.* **127**, 221106 (2007).
61. G. Knizia, T. B. Adler, H.-J. Werner, Simplified CCSD (T)-F12 methods: Theory and benchmarks. *J. Chem. Phys.* **130**, 054104 (2009).
62. K. A. Peterson, T. B. Adler, H.-J. Werner, Systematically convergent basis sets for explicitly correlated wavefunctions: The atoms H, He, B–Ne, and Al–Ar. *J. Chem. Phys.* **128**, 084102 (2008).
63. M. Valiev, E. J. Bylaska, N. Govind, K. Kowalski, T. P. Straatsma, H. J. J. Van Dam, D. Wang, J. Nieplocha, E. Apra, T. L. Windus, W. A. de Jong, NWChem: A comprehensive and scalable open-source solution for large scale molecular simulations. *Comput. Phys. Commun.* **181**, 1477–1489 (2010).
64. X. Hu, W. L. Hase, T. Pirraglia, Vectorization of the general Monte Carlo classical trajectory program VENUS. *J. Comput. Chem.* **12**, 1014–1024 (1991).
65. U. Lourderaj, R. Sun, S. C. Kohale, G. L. Barnes, W. A. de Jong, T. L. Windus, W. L. Hase, The VENUS/NWChem software package. Tight coupling between chemical dynamics simulations and electronic structure theory. *Comput. Phys. Commun.* **185**, 1074–1080 (2014).
66. P. M. Rodger, On the accuracy of some common molecular dynamics algorithms. *Mol. Simul.* **3**, 263–269 (1989).
67. W. C. Swope, H. C. Andersen, P. H. Berens, K. R. Wilson, A computer simulation method for the calculation of equilibrium constants for the formation of physical clusters of molecules: Application to small water clusters. *J. Chem. Phys.* **76**, 637–649 (1982).
68. Y. Luo, K. Fujioka, A. Shoji, W. L. Hase, K.-M. Weitzel, R. Sun, Theoretical study of the dynamics of the $HBr^+ + CO_2 \rightarrow HOCO^+ + Br$ reaction. *J. Phys. Chem. A* **124**, 9119–9127 (2020).
69. R. Krishnan, J. S. Binkley, R. Seeger, J. A. Pople, Self-consistent molecular orbital methods. XX. A basis set for correlated wave functions. *J. Chem. Phys.* **72**, 650–654 (1980).
70. F. Weigend, R. Ahlrichs, Balanced basis sets of split valence, triple zeta valence and quadruple zeta valence quality for H to Rn: Design and assessment of accuracy. *Phys. Chem. Chem. Phys.* **7**, 3297–3305 (2005).

Acknowledgments: A.V. and R.S. thank the Information Technology Service (ITS) from the University of Hawai'i at Mānoa for the computational resources. **Funding:** The work at the University of Hawai'i at Mānoa was supported by the US National Science Foundation (CHE-2244717). M.X.S. and B.R.L.G. acknowledge financial support from Conselho Nacional de Desenvolvimento Científico e Tecnológico (CNPq, grant numbers 311508/2021-9 and 405524-2021-8) and Fundação de Amparo à Pesquisa e Inovação do Espírito Santo (FAPES).
Author contributions: Conceptualization: S.J.G. and R.I.K. Formal analysis: S.J.G., A.V., and M.X.S. Funding acquisition: R.I.K., B.R.L.G., and R.S. Investigation: S.J.G., Z.Y., A.V., and M.X.S. Software: A.V. and M.X.S. Supervision: R.I.K., B.R.L.G., and R.S. Visualization: S.J.G. Writing—original draft: S.J.G., A.V., and M.X.S. Writing—review and editing: S.J.G., R.I.K., B.R.L.G., and R.S.
Competing interests: The authors declare that they have no competing interests. **Data and materials availability:** All data needed to evaluate the conclusions in the paper are present in the paper and/or the Supplementary Materials.

Submitted 16 May 2024
Accepted 11 October 2024
Published 15 November 2024
10.1126/sciadv.adq5018